CARBON 47 (2009) 2239–2243

available at www.sciencedirect.com

ScienceDirect

journal homepage: www.elsevier.com/locate/carbon

A neutron diffraction study of nano-crystalline graphite oxide

J.A. Johnson[a,b,*], C.J. Benmore[b], S. Stankovich[c], R.S. Ruoff[d]

[a]University of Tennessee Space Institute, MSE, 411 B.H. Goethert Parkway, Tullahoma, TN 37388, USA
[b]Argonne National Laboratory, Argonne, IL 60439, USA
[c]Northwestern University, Evanston, IL, USA
[d]Department of Mechanical Engineering and the Texas Materials Institute, The University of Texas, 1 University Station C2200, Austin, TX 78712, USA

ARTICLE INFO

Article history:
Received 27 January 2009
Accepted 9 April 2009
Available online 21 April 2009

ABSTRACT

The structure of graphite oxide has been studied by neutron diffraction and is found to be nano-crystalline, the diffraction pattern being a mixture of Bragg and diffuse scattering. Three strong Bragg peaks were found in the structure factor from which the layer spacing was calculated and found to be consistent with different structural regions within the graphite oxide, specifically regions of graphitic-like flat hexagons and regions containing oxidized chain-like structures. The neutron scattering pair distribution function is compared to four previously published low energy Monte Carlo structural models of GO.

1. Introduction

Graphite oxide (GO) was first prepared in the mid-19th century [1,2] but its precise structure is still uncertain. The structure has been studied since the 1930s and several models have been proposed [3–6] but they remain controversial. The structure of GO is of interest, especially the nature of the functional groups, as GO has a variety of potential uses, such as for the positive electrode in primary lithium cells [7–9]. The expanded interlayer distance also allows the ions to more easily intercalate. Mermoux et al. [10] and He et al. [11] have confirmed the existence of a C–OH group by NMR. He et al. also presented strong evidence of epoxide (1,2-ether) groups, which they claim are responsible for the strong oxidizing properties of GO. Lerf et al. [12] and He et al. [11] determined that the structure of GO contains two kinds of regions: aromatic regions with unoxidized benzene rings and regions containing aliphatic six-membered rings; the relative amounts of these two regions depend on the degree of oxidation. A more recent paper [13] has given evidence of graphitic AB stacking order of GOs and a hexagonal structure in the plane with functional groups such as hydroxyl, epoxide, carbonyl, and some randomly distributed alkyl groups. This graphitic-layered structure has been confirmed by C 1*s* X-ray absorption spectroscopy (XAS) [14] as has the type and position of various functional groups.

Since GO is heterogeneous, the total neutron scattering data presented in this paper gives a statistically averaged structure for the large volume sample (~3 cm^3) studied. The measured pair distribution function is compared to previously published models of low energy GO structures.

2. Experimental

2.1. Sample preparation

Graphite oxide was prepared according to the Hummers method [15]. Graphite (10 g) was suspended into cold (0 °C, ice bath) concentrated sulfuric acid (230 mL) in a 1 L

* *Corresponding author:* Address: University of Tennessee Space Institute, MSE, 411 B.H. Goethert Parkway, Tullahoma, TN 37388, USA. Fax: +1 931 393 7437.
E-mail address: jjohnson@utsi.edu (J.A. Johnson).
0008-6223/$ - see front matter
doi:10.1016/j.carbon.2009.04.016

round-bottom flask equipped with a mechanical stirring rod. Potassium permanganate ($KMnO_4$, 30 g) was then added gradually with stirring and cooling so that the temperature did not exceed 20 °C. The stirring was then continued for 2 h at 35 °C, followed by the addition of distilled water (460 mL) and stirred for an additional 15 min. Finally the content of the flask was poured into distilled water (1.40 L) and a sufficient amount of hydrogen peroxide (30% solution in water) was added to destroy the excess of permanganate (indicated by a color change from dark brown to yellow). Graphite oxide was isolated by filtration through a sintered glass filter and washed with a solution of HCl in water (1:10 v/v dilution from commercial concentrated HCl (12.1 N)) until sulfates were no longer detected in the filtrate.

2.2. *Diffraction measurements*

Pulsed neutron diffraction measurements were made on the glass, liquids and amorphous materials diffractometer (GLAD) at the intense pulsed neutron source (IPNS) at Argonne National Laboratory (ANL). The GO sample was contained in a thin-walled (0.1 mm) vanadium can with an inner radius of 9.3 mm. The relative humidity inside the can was ambient, which is generally ~45% in the air-conditioned controlled atmosphere at IPNS. The data analysis was performed using the *ISAW* software package for time-of-flight neutron diffraction data [16]. This suite of programs enables data corrections to be made for container scattering, attenuation, multiple scattering and heavy atom inelastic scattering and the corrected data are normalized to the scattering from a vanadium rod. The neutron scattering lengths were obtained from the tabulated values of Sears [17]. A low (4th) order polynomial was used to remove the small amount of hydrogen scattering, using the procedure described by Soper and Luzar [18] see Fig. 1. Data were collected using momentum transfers (Q) from 0.3 up to 40 $Å^{-1}$ and after analysis yielded the static structure factor, S(Q):

$$S(Q)-1=\frac{I(Q)}{\left[\sum_i c_i b_i(Q)\right]^2}=\frac{\sum_{ij} c_i b_i(Q) c_j b_j(Q)(S_{ij}(Q)-1)}{\left[\sum_i c_i b_i(Q)\right]^2}$$

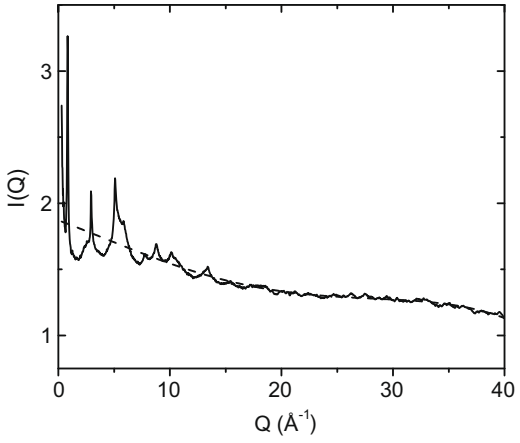

Fig. 1 – Measured neutron intensity (solid line) with slope due to hydrogen scattering approximated by a 4th order polynomial fit (dashed line).

where c_i is the concentration of species *i* and b_i is the coherent scattering length for neutrons. For GO it is expected that the dominant contribution will come from the C–C partial structure factor. A detailed structure of graphite oxide has not previously been resolved using total scattering methods, in part because of variations in the exact composition, c_i, and the density of the material, making precise data corrections and a quantitative analysis problematic. Typically, long wavelength errors in the attenuation and multiple scattering corrections due to these uncertainties lead to (unphysical) artifacts below ~1 Å in real space, but total scattering data are generally robust at longer (physically meaningful) distances. To circumvent the normalization problem due to the variation in composition and density, the S(Q) was scaled until the unphysical low-*r* features in the radial distribution function G(*r*) oscillated around zero; a necessary condition if these parameters were known.

The S(Q) is related to the total differential distribution function $D(r) = 4\pi\rho r G(r)$ via a Fourier transform, given by [19]:

$$S(Q)=1+\frac{1}{Q}\int_0^\infty dr D(r)\sin(Qr)$$

D(*r*) has the advantage that ρ, the atomic number density, is not required in the Fourier transform but it still yields structural information in terms of peak positions of all the atom–atom correlations. A Lorch modification function was used to reduce termination effects associated with the momentum transfer cutoff at Q_{max}, which in this case is 30 $Å^{-1}$. Statistical accuracy degrades with increasing Q due to the decreasing detector solid angle coverage. However, truncating the data at lower Q values can introduce Fourier ripples, particularly at low-*r*, which overlap with the shortest (e.g. O–H and C–H bond) distances.

3. Results and discussion

The static structure factor S(Q) is shown in Fig. 2 up to 40 $Å^{-1}$ with an expanded scale inset up to 10 $Å^{-1}$. There are three strong Bragg peaks at Q = 0.825 ± 0.01, 2.93 ± 0.01 and

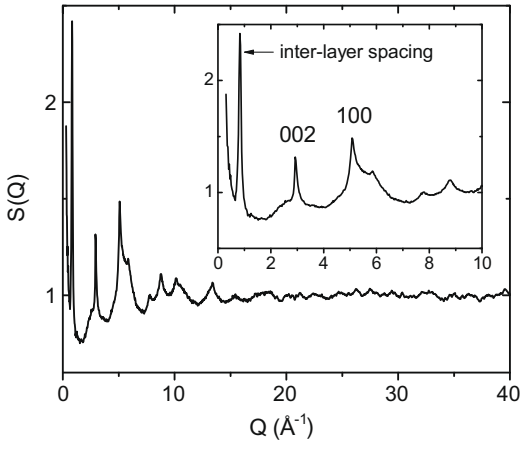

Fig. 2 – The corrected neutron structure factor for nanocrystalline GO, normalized as described in text. The insert highlights three Bragg peaks and diffuse scattering in the low-Q region.

5.08 ± 0.01 Å^{-1} together with a considerable degree of diffuse scattering extending out to high-Q. The rise towards the lowest Q-values below 0.4 Å^{-1} indicates longer range density fluctuations, with a minimum periodicity of ~15 Å (2 layers), consistent with the notion of different regions within the GO structure. The Q = 0.825 Å^{-1} peak corresponds to the inter-layer spacing between planes in GO with a periodicity of 7.62 Å and has a full width half maximum of 0.10 Å^{-1}. This interlayer separation, per XRD studies, corresponds to a relative humidity of 40–45% [5,20], consistent with the controlled atmosphere at IPNS. GO has interlamellar water and is a swellable material based on relative humidity. The 2.93 Å^{-1} peak corresponds to the 002 peak in graphite [21] and the peak at 5.08 Å^{-1} is the 100 reflection.

Fig. 3 shows the neutron differential distribution function, $D(r)$, showing the local structure. The first real peaks are seen at 1.48 ± 0.01 Å and 2.51 ± 0.01 Å. Jeong et al. [14] performed a study on graphite oxide using X-ray absorption spectroscopy (XAS) and were able to decipher the percentage contribution to the different bonds within the sample. To the nearest percent these are given as C–C (55%); C–OH (21%); C–O–C (18%); and HO–C=O (6%). It is known from previous diffraction studies [22] that the C–C bond distance is ~1.50 ± 0.01 Å in semi-crystalline materials and the C–O distance is ~1.43 ± 0.01 Å. As the peak at 1.48 Å is somewhat asymmetric it is likely that it contains contributions from both of these correlations. According to [14] there are no direct C–H bonds, which would be seen at ~1.10 ± 0.01 Å. We note that since the coherent neutron scattering length of hydrogen is negative, C–H correlations appear as a dip in $D(r)$. Fig. 2 in [14] gives a schematic model of GO where the oxygen and hydroxyl groups are located randomly above and/or below the carbon basal plane with carboxyl and alkyl groups at the edge of the GO flakes. With this structure in mind it is likely that the next definite peak at 2.51 Å is associated with the next nearest carbon on the GO flake. In regular graphite, carbon atoms are arranged in hexagonal rings with internal angles of 120°. Given that the distance between the carbon atoms in this paper is close to 1.48 Å, the distance between the next nearest carbon atoms is $2 \times 1.48 \times \sin 60° = 2.56$ Å, close to where the second definitive peak is seen, as shown in Fig. 3. The fact that the match between the calculation and experiment is not exact is probably due to some mixing of C–O bonding into the peak.

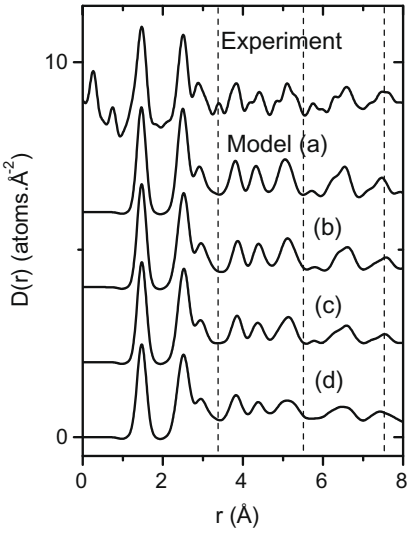

Fig. 3 – The measured neutron differential distribution function for nano-crystalline GO (top curve) showing the local structure. This is compared to the same functions calculated for various Monte Carlo models of low energy GO structures published in [23]: (a) a disordered but pristine sheet; (b) a sheet containing a one-atom vacancy defect; (c) a sheet containing a two atom vacancy defect and (d) a sheet containing a hole created by removing a hexagonal unit of carbon atoms. The model data were artificially convoluted with a Gaussian function of root mean squared displacement, 0.25 Å, to give similar peak widths to the experimental data. The dashed lines are drawn to highlight the location of some representative peaks (see text).

Computational studies of the structure of GO have been performed by Paci et al. [23]. This group [23] decorated graphene sheets with a variety of functional groups using a Monte Carlo method and we have calculated the corresponding neutron total differential distribution function for four of these published models (shown in Fig. 3 of [23]) using the formalism described earlier. The results of the model low energy GO structures are shown in Fig. 3. Model (a) describes a disordered but pristine sheet, (b) has a one-atom vacancy obtained by removing a carbon atom from the center of the sheet (c) a two atom vacancy obtained by removal of a second atom adjacent to the first, and (d) a large hole defect generated by removing an entire hexagonal unit of carbon atoms. As expected the experimental data show more detailed structure compared to these idealized models. Nonetheless the pristine hexagonal structure agrees reasonably well with the measured data accounting for many of the peaks and their relative intensities within the first layer. Differences between the models appear mostly as peak shifts and intensity changes with the peaks broadening significantly at higher-r, notably at 5.08 and 7.49 Å, as more defects are added. Model (d) has considerably broader peaks than the experimental data, suggesting that if holes do occur they have a very low concentration. The best agreement is obtained with the one and two vacancy models, i.e. 1 or 2 defects per ~126 carbon atoms. Unfortunately none of the models are able to predict the origin of the 3.36 Å peak observed in the neutron data. However, this does coincide exactly with the inter-layer spacing in high quality graphite and could be some un-reacted graphite.

Fig. 4 shows the function $rD(r)$ to emphasize the high-r structure which describes, in part, atom–atom correlations in the second layer of the GO structure. The varying composition of GO makes quantitative atomic modeling of nanometer-ranged interactions difficult. Indeed, of six structural models proposed for GO, the two which have been recently identified as the most consistent with ^{13}C NMR data consist of two distinct regions [24]. The Lerf–Klinowski model has aromatic regions of unoxidized benzene rings and regions of aliphatic six-membered rings. The Szabo et al. model has regions of trans-linked cyclohexane chains and regions containing ribbons of flat hexagons. Since both models contain some remnant of the original graphite layer building block, we compare an $rD(r)$ function with atom–atom correlations

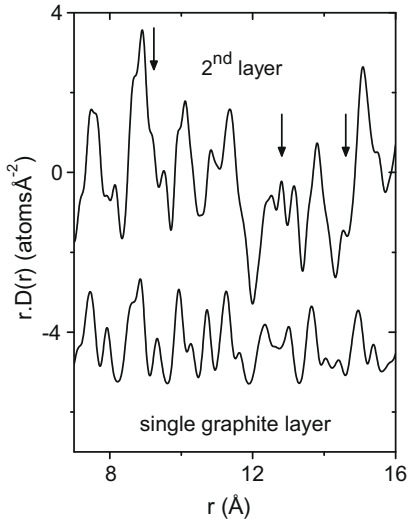

Fig. 4 – Differential distribution function *D*(*r*) multiplied by *r*, to emphasize the atom–atom correlations over the region of the second layer, as defined by the 7.62 Å periodicity given by the first Bragg peak in the structure factor. The bottom curve shows the same function for a perfect single crystalline graphite layer (scaled and broadened by 0.5 Å for clarity). The arrows indicate peaks which appear absent from single layer model graphite correlations.

arising from a single graphite plane of hexagons in Fig. 4. In the graphite single layer model the root mean square deviations have been artificially broadened to 0.5 Å. We find that in the second layer (i.e. between 7.62 and 15.24 Å) different relative peak intensities occur due to additional inter-layer interactions and changes due to oxidation. More importantly, several new peaks or shoulders appear, including ones at 9.2, 12.8 and 14.6 Å not present in the single graphite layer. While the neutron diffraction data may not yield the explicit structure from which these correlations arise, we note that any atomic scale model must contain these features to be viable.

The mixture of Bragg and diffuse scattering is indicative of a nano-crystalline material. For regions of varying density and composition this could be described by an amorphous phase containing small grains of crystalline material within it. Generally, nano-crystalline materials differ from polycrystalline materials as the latter consist solely of crystalline grains separated by grain boundaries; as the size of the crystallites reduces an increasing portion are found on the grain boundaries. At roughly 5 nm ~50% of the material will be grain boundaries. The development of nano-crystalline materials is in its infancy but significant growth is expected for structural materials and coatings.

4. Conclusions

The inter-layer spacing of GO has been measured directly from the low-Q Bragg peak and found to be at $Q = 0.825 \pm 0.01$ Å^{-1}. The real space neutron data is consistent with models which suggest GO has regions of graphitic-like hexagons and regions containing oxidized chain-like structures. The data are largely consistent with recently published one and two atom vacancy models but not with models showing larger holes, indicating that if these exist they must have a relatively low concentration. The neutron data also show additional correlations, particularly at 3.36 Å, not predicted by these models but it could be attributed to un-reacted graphite.

Acknowledgements

Dr. J. Paci is thanked for providing the atomic coordinates of the models in Ref. [23]. The experiments at Argonne National Laboratory were supported by the US. DOE under contract number DE-AC02-06CH11357. RSR appreciates support from the DARPA iMINT and The University of Texas at Austin.

REFERENCES

[1] Brodie BC. Note sur un nouveau procédé pour la purification et la désagrégation du graphite. Ann Chim Phys 1855;45:351–3.
[2] Brodie BC. On the atomic weight of graphite. Philos Trans R Soc (London) A 1859;149:249–59.
[3] Hofmann U, Frenzel A, Csalan. The constitution of graphite acid and its reactions. Liebigs Ann Chem 1934;510:1–4.
[4] Ruess G. Über das graphitoxyhydroxyd (graphitoxyd). Monatsh Chem 1946;76:381–417.
[5] Scholtz W, Boehm HP. Untersuchungen am graphitoxid. VI. Betrachtungen zur struktur des graphitoxids. Anorg Allg Chem 1969;396:327–40.
[6] Nakajima T, Matsuo Y. Formation process and structure of graphite oxide. Carbon 1994;32(3):469–75.
[7] Cassagneau T, Fendler JH. High density rechargeable lithium-ion batteries self-assembled from graphite oxide nanoplatelets and polyelectrolytes. Adv Mater 1998;10(11):877–81.
[8] Du X, Xiao M, Meng Y, Hay A. Direct synthesis of poly(arylenedisulfide)/carbon nanosheet composites via the oxidation with graphite oxide. Carbon 2005;43:195–7.
[9] Matsuo Y, Higashika S, Kimura K, Miyamoto Y, Fukutsuka T, Sugie Y. J Mater Chem 2002;12:1592–6.
[10] Mermoux M, Chabre Y, Rousseau A. FTIR and C-13 NMR-study of graphite oxide. Carbon 1991;29(3):469–74.
[11] He HY, Klinowski J, Forster M, Lerf A. A new structural model for graphite oxide. Chem Phys Lett 1998;287(1–2):53–6.
[12] Lerf A, He HY, Forster M, Klinowski J. Structure of graphite oxide revisited. J Phys Chem B 1998;102(23):4477–82.
[13] Jeong HK, Lee YP, Lahaye R, Park MH, An KH, Kim IJ, et al. Evidence of graphitic AB stacking order of graphite oxides. J Am Chem Soc 2008;130(4):1362–6.
[14] Jeong H-K, Noh H-J, Kim J-Y, Jin MH, Park CY, Lee YH. X-ray absorption spectroscopy of graphite oxide. Europhys Lett 2008;82:67004.
[15] Hummers WS, Offeman RE. Preparation of graphite oxide. J Am Chem Soc 1958;80:1339.
[16] Tao J, Bertmore CJ, Worlton TG, Carpenter JM, Mikkelson D, Mikkelson R, et al. Time-of-flight neutron total scattering data analysis implemented in the software suite ISAW. Nucl Instrum Methods Phys Res Sect A – Accel Spectrom Dect Assoc Equip 2006;562(1):422–32.
[17] Sears VF. Methods of experimental physics. vol. 23. New York: Academic Press; 1986. p. 521–49.

[18] Soper A, Luzar A. A neutron diffraction study of dimethyl sulphoxide–water mixtures. J Chem Phys 1992;97:1320–31.
[19] Keen DA. A comparison of various commonly used correlation functions for describing total scattering. J Appl Crystallogr 2001;34:172–7.
[20] Lerf A, Buchsteiner A, Pieper J, Schöttl S, Dekany I. Hydration behavior and dynamics of water molecules in graphite oxide. J Phys Chem Solids 2006;67:1106–10.
[21] Trucano P, Chen R. Structure of graphite by neutron-diffraction. Nature 1975;258(5531):136–7.
[22] Johnson JA, Saboungi ML, Price DL, Ansell S, Russell TP, Halley JW, et al. Atomic structure of solid and liquid polyethylene oxide. J Chem Phys 1998;109(16):7005–10.
[23] Paci JT, Belytschko T, Schatz GC. Computational studies of the structure, behavior upon heating, and mechanical properties of graphite oxide. J Phys Chem C 2007;111(49):18099–111.
[24] Cai W, Piner R, Stadermann FJ, Park S, Shaibat MA, Ishii Y, et al. Synthesis and solid-state NMR structural characterization of 13C-labeled graphite oxide. Science 2008;321:1815–7.